eNeuro

Research Article: New Research | Disorders of the Nervous System

Longitudinal effects of ketamine on dendritic architecture in vivo in the mouse medial frontal cortex,,

Ketamine and structural plasticity

Victoria Phoumthipphavong[1], Florent Barthas[1], Samantha Hassett[1] and Alex C. Kwan[1,2]

[1]*Department of Psychiatry, Yale University, New Haven, Connecticut*

[2]*Department of Neuroscience, Yale University, New Haven, Connecticut*

DOI: 10.1523/ENEURO.0133-15.2016

Received: 6 November 2015

Revised: 13 March 2016

Accepted: 15 March 2016

Published: 23 March 2016

Author Contributions: V.P. and A.C.K. designed research; V.P. and F.B. performed research; V.P., S.H., and A.C.K. analyzed data; V.P. and A.C.K. wrote the paper.

Funding: NARSAD Young Investigator Award; Golden Rule Family Foundation;

Conflict of Interest: Authors report no conflict of interest.

Correspondence: Alex C. Kwan, Ph.D., Department of Psychiatry, Yale University, 300 George St Suite 901, New Haven, CT 06511, E-mail: alex.kwan@yale.edu.

Cite as: eNeuro 2016; 10.1523/ENEURO.0133-15.2016

eNeuro

http://eneuro.msubmit.net

eN-NWR-0133-15R3

Longitudinal effects of ketamine on dendritic architecture in vivo in the mouse medial frontal cortex

1. Manuscript Title: Longitudinal effects of ketamine on dendritic architecture in vivo in the mouse medial frontal cortex

2. Abbreviated Title: Ketamine and structural plasticity

3. Authors and Affiliations:
Victoria Phoumthipphavong, Florent Barthas, Samantha Hassett, Alex C. Kwan
Department of Psychiatry (VP, FB, SH, ACK); and the Department of Neuroscience (ACK), Yale University, New Haven, Connecticut

4. Author Contributions: VP and ACK designed research. VP and FB performed research. VP, SH, and ACK analyzed data. VP and ACK wrote the paper.

5. Correspondence should be addressed to:
Alex C. Kwan, Ph.D.
Department of Psychiatry, Yale University
300 George St Suite 901, New Haven, CT 06511
Email: alex.kwan@yale.edu.

6. Number of Figures: 6
7. Number of Tables: 1
8. Number of Multimedia: 0
9. Number of words for Abstract: 242
10. Number of words for Significance: 118
11. Number of words for Introduction: 604
12. Number of words for Discussion: 1,281

13. Acknowledgements. We thank Ronald Duman and George Aghajanian for helpful discussions, William Cafferty for providing mice for pilot experiments, and Jaime Grutzendler for mice and advice on the surgery.

14. Conflict of Interest. Authors report no conflict of interest.

15. Funding Sources. This work was supported by a NARSAD Young Investigator Award (ACK), and the Golden Rule Family Foundation (ACK).

Longitudinal effects of ketamine on dendritic architecture in vivo in the mouse medial frontal cortex

Abstract

A single subanesthetic dose of ketamine, an N-methyl-D-aspartate receptor antagonist, leads to fast-acting antidepressant effects. In rodent models, systemic ketamine is associated with higher dendritic spine density in the prefrontal cortex, reflecting structural remodeling that may underlie the behavioral changes. However, turnover of dendritic spines is a dynamic process *in vivo*, and longitudinal effects of ketamine on structural plasticity remain unclear. The purpose of the current study is to use subcellular-resolution optical imaging to determine the time course of dendritic alterations *in vivo* following systemic ketamine administration in mice. We used two-photon microscopy to visualize repeatedly the same set of dendritic branches in the mouse medial frontal cortex (MFC) before and after a single injection of ketamine or saline. Compared to controls, ketamine-injected mice had higher dendritic spine density in MFC for up to 2 weeks. This prolonged increase in spine density was driven by an elevated spine formation rate, and not changes of the spine elimination rate. A fraction of the new spines following ketamine injection was persistent, indicative of functional synapses. In a few cases, we also observed retraction of distal apical tuft branches on the day immediately after ketamine administration. These results indicate that following systemic ketamine administration, certain dendritic inputs in MFC are removed immediately while others are added gradually. These dynamic structural modifications are consistent with a model of ketamine action in which the net effect is a re-balancing of synaptic inputs received by frontal cortical neurons.

Significant Statement

A single dose of ketamine leads to fast-acting antidepressant effects, and thus understanding its mechanism of action would facilitate the development of new treatments for mood disorders. One potential mechanism is the remodeling of synaptic connections, because ketamine administration in rodents leads to a higher density of dendritic spines in the frontal cortex. Structural remodeling, however, is a dynamic process and the longitudinal effects of ketamine are poorly understood. In this study, we used cellular-resolution optical imaging methods to repeatedly visualize dendritic spines from the same set of neurons for >2 weeks in the mouse frontal cortex. The results are consistent with a model of action for ketamine involving the re-balancing of synaptic inputs in the frontal cortex.

73 **Introduction**

74 Major depressive disorder is a top contributor to disease burden among mental illnesses
75 in the United States (US Burden of Disease Collaborators, 2013). Core symptoms for
76 depressive disorders are debilitating, yet treatment options are limited. Typical
77 antidepressants require several weeks to months to be effective, and approximately one
78 third of patients remain nonresponsive even after multiple trials. In contrast to the slow
79 onset of action for the currently available antidepressants, a single dose of ketamine
80 produces antidepressant effects within several hours (Berman et al., 2000) and can last
81 for up to two weeks (Ibrahim et al., 2012). Studies of ketamine effects in animal models
82 have found antidepressant-like behavioral responses in naive and stressed rodents (Li et
83 al., 2010; Autry et al., 2011; Li et al., 2011; Donahue et al., 2014). These studies have
84 shed light on the molecular signaling pathways recruited by systemic ketamine
85 administration. However, still unclear are the cellular and network mechanisms
86 responsible for the behavioral improvements (Sanacora and Schatzberg, 2015).
87
88 One striking consequence of systemic ketamine administration in naive rodents is an
89 increase in the dendritic spine density in the distal and proximal tufts of layer 5 pyramidal
90 neurons in the medial prefrontal cortex (Li et al., 2010; Liu et al., 2013; Ruddy et al.,
91 2015). These observations of synaptogenesis are in stark contrast with the structural
92 and synaptic atrophy reported for patients with major depression (Drevets et al., 1997;
93 Kang et al., 2012) and chronic stress models (Cook and Wellman, 2004; Radley et al.,
94 2004; Liston et al., 2006; Christoffel et al., 2011). The opposing effects of ketamine and
95 stress on neural architecture suggest that there could be a structural basis for
96 antidepressant actions. Namely, fast-acting antidepressants such as ketamine may
97 restore synaptic connections that were lost in stress and mood disorders (Duman and
98 Aghajanian, 2012). Indeed, when chronically stressed rats were injected with a single

dose of ketamine, the stress-induced reduction in dendritic spine density could be reversed (Li et al., 2011).

However, the turnover of dendritic spines is a dynamic process *in vivo*. An increase in dendritic spine density could be due to an increase in formation rate, a decrease in elimination rate, or a combination of both factors. Moreover, newly formed spines can be transient or persistent, either disappearing or stabilizing after several days. It is unknown whether new spines following systemic ketamine are persistent and thus associated with functional synapses (Knott et al., 2006). Characterizing these dynamics requires longitudinal methods. Two-photon microscopy is an optical imaging technique that enables visualization of dendritic architecture *in vivo* at subcellular resolution for up to several months (Grutzendler et al., 2002; Holtmaat et al., 2009). This approach has been used to investigate structural plasticity following sensory experience (Trachtenberg et al., 2002), learning (Fu et al., 2012; Lai et al., 2013), and exposure to substances including corticosterone (Liston and Gan, 2011) and cocaine (Muñoz-Cuevas et al., 2013).

In this study, we used two-photon imaging to characterize the effects of a single, subanesthetic dose of ketamine on the dendritic architecture in the mouse medial frontal cortex (MFC). Our results showed that systemic ketamine leads to a relative increase in dendritic spine density, a prolonged change driven by an elevated rate of spine formation. A fraction of the ketamine-induced new spines was persistent and could be observed after 4 days, indicative of functional synapses. Unexpectedly, we also observed a loss of distal apical tuft branches that occurred specifically and immediately on the day after ketamine administration. These data demonstrate distinct short- and long-term consequences of ketamine on dendritic architecture, and highlight its impact on modifying the synaptic inputs impinging on frontal cortical neurons.

125

126 **Methods and Materials**

127 **Mice.** All animal procedures were performed in accordance with the Yale University
128 animal care committee's regulations. Experiments were performed on adult (postnatal
129 day 73 – 149) *Thy1-GFP-M* (n = 13; #007788, Jackson Laboratory,
130 RRID:IMSR_JAX:007788) and *Thy1-YFP-H* transgenic mice (n = 3; #003782, Jackson
131 Laboratory, RRID:IMSR_JAX:003782). Mice of both sexes were used. Mice were
132 housed under controlled temperature on a 12/12-hr light-dark cycle with siblings (1-5 per
133 cage) and nesting material.

134

135 **Surgery.** Anesthesia was induced with a 2% isoflurane and oxygen mixture, which was
136 lowered to 1.5% for the remainder of the surgery. Mice were secured by ear bars in a
137 stereotaxic frame. Their body temperature was regulated with a hot water circulation
138 pad. Mice were injected with carprofen (5 mg/kg, s.c., 024751, Butler Animal Health) and
139 dexamethasone (40 mg/kg, i.m., D4902, Sigma-Aldrich) prior to surgery. A 2 to 3-mm
140 diameter craniotomy was made over the right medial frontal cortex with a handheld
141 dental drill. After the skull was carefully removed, the surface of the brain was irrigated
142 with an artificial cerebral spinal fluid (ACSF; in mM: 5 KCl, 5 HEPES, 135 NaCl, 1
143 MgCl2, 1.8 CaCl2; pH 7.3) until bleeding subsides. A drop of warmed, low melting-point
144 agarose solution (2% in ACSF, Type II-A, High EEO, A9793, Sigma-Aldrich) was applied
145 over the craniotomy. A two-layer glass plug was fabricated by first etching out a 2-mm
146 diameter circle from a #0 thickness glass coverslip, then bonded with UV-activated
147 epoxy (NT37-322, Edmund Optics) to a #1 thickness, 3-mm diameter round glass
148 coverslip (64-0720-CS-3R, Warner Instruments). The glass plug was placed over the
149 craniotomy and held in place until the agarose solidifies. The glass plug was then
150 stabilized by applying light pressure and adding super glue around the edges. A

151 stainless steel head plate was affixed to the skull using Metabond (C&B, Parkell Inc.).
152 Mice were given another dose of carprofen (5 mg/kg, s.c.) immediately after surgery and
153 for each of the following 3 days (5 mg/kg, i.p.). Mice were given a period of at least 3
154 weeks to recover before imaging begins.
155
156 **Imaging.** Mice were anesthetized with 1.5% isoflurane and head-fixed. Temperature
157 was regulated using a heating pad with rectal probe feedback. The two-photon
158 microscope (Movable objective microscope, Sutter) was controlled using the ScanImage
159 software (Pologruto et al., 2003, RRID:SCR_014307). Excitation was provided by an
160 ultrafast laser (Chameleon Ultra II, Coherent) and focused with a high-numerical
161 aperture microscope objective (XLUMPLFLN20X/1.0, Olympus). For imaging GFP- or
162 YFP-expressing dendrites, excitation wavelength was set at 920 nm, and emission was
163 collected behind a bandpass filter from 475 – 550 nm. Each mouse was injected with
164 either ketamine (10 mg/kg, i.p.) or saline vehicle on a non-imaging day. To investigate
165 short-term effects, mice were imaged on -3, -1, and 1 day relative to the day of injection.
166 For long-term studies, mice were imaged on -3, -1, 1, 3, 5, 10, and 15 day relative to the
167 day of injection. Multiple fields of view were imaged in the same mouse. The same field
168 of view was identified across days by finding landmark structures such as blood vessels
169 or an edge of the glass window. At each field of view, image stacks were acquired at
170 1024 x 1024 pixels, spanning a field of view 60.5 x 60.5 μm, and at 2 μm steps for a z-
171 range of 20 – 30 μm. Each imaging session lasted up to 2.5 hr. Although we did not
172 explicitly record the duration of imaging sessions, we estimated post hoc based on the
173 acquisition times of the first and last image files in the computer.
174
175 **Image analysis.** For all the figures, we are presenting the raw images with only
176 adjustments to the black and white levels (linear), with no modification to contrast (non-

177 linear) or removal of neighboring axons or any other manipulations. Initially, image
178 stacks were processed for motion correction using the StackReg plug-in (Thévenaz et
179 al., 1998, RRID:SCR_014308) in ImageJ (Schneider et al., 2012, RRID:SCR_003070).
180 Then, structural parameters were analyzed from each image stack using ImageJ. The
181 physical parameters of dendritic spines were characterized based on criteria established
182 in a standardized protocol (Holtmaat et al., 2009). Briefly, dendritic spines were counted
183 if the protrusions extend at least 0.4 μm away from the shaft. Dendritic spine length was
184 the distance from the base at the shaft to the tip. Dendritic spine head diameter was the
185 width at the widest extent of the spine. Distances were measured using the line segment
186 tool in ImageJ. The dendritic spine formation rate was defined as the number of new
187 spine protrusions observed in two consecutive imaging sessions divided by the total
188 number of dendritic spines in the first imaging session. To assess longitudinal changes
189 of spine formation rate, we calculated the difference from baseline by subtracting the
190 formation rate of each field of view by the baseline rate of the subject. The baseline rate
191 of each subject was estimated by averaging the spine formation rates of all fields of view
192 imaged from the same individual prior to injection, i.e. between day -3 and -1. The
193 dendritic elimination rate was quantified using the same procedure for spine protrusions
194 that disappeared. Most of the sessions were imaged 2 days apart, but some sessions
195 were imaged 5 days apart (i.e. day 5-10 and day 10-15). Presumably, with the same
196 spine formation rate, we would observe more new spines in 5-day-apart sessions
197 relative to 2-day-apart sessions because more time has elapsed. Therefore, when
198 estimating the spine formation/elimination rate from new/lost spine counts, we report
199 turnover rates for 5-day-apart sessions with a correction factor, by multiplying the
200 measured rates by 2/5. For the apical tuft branches, dendritic segments were traced
201 over using the freehand line tool, and then summed for total length in ImageJ. To assess
202 longitudinal changes of the imaged dendritic segments, we calculated the fold-change

from last session for each field of view, by dividing the measured branch length of an imaging session by that of the prior imaging session.

Statistics. We performed statistical tests considering fields of view as independent samples. This is a major assumption, justified in part by the fact that the fields of view were at random, non-overlapping locations and each one comprises of a very small portion (0.06%) of the window area of each mouse. The reason for making this assumption is that a different number of fields of view was taken for each mouse, so if we compare subjects only, the results will have a bias for those with fewer fields of view. To ensure that this assumption does not affect the major conclusions of the paper, we repeated statistical tests for 3-session data considering each mouse as a sample when possible. For all longitudinal results, two-way mixed analysis of variance (ANOVA) with repeated measures was used to test the factors contributing to changes in spine density, dendritic branch length, spine formation rate, and spine elimination rate. The factors were treatment (ketamine or saline; between-subject), day (within-subject), and their interaction. The two-tailed t-test was used to compare means that did not involve multiple days. The two-sample Kolmogorov-Smirnov test was used to compare cumulative distributions. Data are reported as mean ± s.e.m. **Table 1** contains a list of the statistical tests performed, observed *p* values, and sample sizes. Observed *p* values and sample sizes are reported instead of observed power to provide more information on the samples involved and because the observed *p* values are directly related to the observed power.

Results

Longitudinal imaging of dendritic architecture in the mouse medial frontal cortex in vivo

To visualize dendritic architecture, we performed two-photon microscopy (**Fig. 1A-B**) using the transgenic *Thy1-GFP-M* and *Thy1-YFP-H* mice (Feng et al., 2000), in which a sparse subset of neocortical neurons expresses the enhanced green or yellow fluorescent protein (GFP and YFP). Many studies have used these mouse lines to investigate structural remodeling, but primarily in the sensory cortices (Trachtenberg et al., 2002; Knott et al., 2006). Therefore, we started by examining the distribution of fluorescent neurons in the frontal cortex. Fluorescence imaging of fixed coronal sections confirmed sparse labeling in anterior cingulate cortex and secondary motor cortex (Cg1 and M2; **Fig. 1C**). In these regions, fluorescence signals originated predominantly from layer 5 pyramidal neurons, as evident from the laminar position of the cell bodies. This is consistent with the knowledge that only deep-layer pyramidal neurons are labeled in these two mouse lines (Feng et al., 2000). Interestingly, although there were no fluorescent cell bodies in the superficial layers, a band of fluorescence signal could be seen in layer 2/3, particularly in the medial regions. This band may arise from axons from other brain regions, such as basolateral amygdala, that send long-range projections to frontal cortical regions (Oh et al., 2014).

In this study, we imaged layer 1 of the medial frontal cortex (MFC), which includes the anterior cingulate cortex (Cg1) and the medial portion of the secondary motor cortex (M2). The choice of MFC was due to practical reasons because two-photon microscopy has depth limitations. Nevertheless, MFC is appropriate for studies of antidepressants as numerous studies have reported stress-induced structural and functional alterations in rodents, either specifically in the cingulate region (Liston et al., 2006; Ito et al., 2010; Kassem et al., 2013) or in a greater region that includes MFC (Radley et al., 2004; 2006; Cerqueira et al., 2007). These results are consistent with a recent brain-wide mapping study, which identified both Cg1 and M2 as regions with significantly reduced activity

levels in a learned helplessness model of depression (Kim et al., 2016). Moreover, mapping of metabolic activity after systemic ketamine showed that MFC is among the activated brain regions in rodents (Duncan et al., 1999; Miyamoto et al., 2000). To prepare for longitudinal *in vivo* imaging, we performed craniotomy above MFC and chronically implanted a ~2-mm-diameter glass window (**Fig. 1D**). After recovery, mice were anesthetized with isoflurane and affixed on head posts under a two-photon microscope. **Figure 1E** shows a low-magnification image of the GFP-expressing dendrites in MFC *in vivo*. For counting dendritic spines, we acquired high-magnification 20 – 30 μm-thick image stacks at multiple fields of view (**Fig. 1F**). Individual dendritic branches could be distinguished from axons by the protruding dendritic spines along the segments. Because we were imaging superficial layers, these neuronal processes represented the distal apical tuft branches of layer 5 pyramidal neurons. We note that all images presented in this paper have only linear adjustments to black and white levels, but are not otherwise altered (see Materials and Methods).

Systemic ketamine administration is associated with higher dendritic spine density in MFC for 2 weeks

To examine the effects of ketamine on structural plasticity in the MFC, we visualized the same fields of view on multiple imaging sessions in adult mice, while administering either a single, subanesthetic dose of ketamine (10 mg/kg, i.p.) or saline vehicle (**Fig. 2A**). We imaged at -3, -1, 1, 3, 5, 10, and 15 day from the injection day. We did not image on the injection day because anesthesia would interfere with neural activity, which is required for the antidepressant effects of ketamine (Fuchikami et al., 2015). We focused on the medial half of the 2-mm-diameter glass window. Image stacks were acquired from multiple, non-overlapping fields of view (60.5 x 60.5 μm), each representing a tiny portion of the window area (0.06%; **Fig. 1D**). In total, we tracked 1665 spines for

281 ketamine (n = 8 mice; 58 fields of view, range = 4 - 21 per mouse) and 3814 spines for
282 saline (n = 8 mice; 97 fields of view, range = 4 – 17 per mouse). All the experiments
283 involved at least the first 3 sessions. In a subset of experiments, we tracked dendritic
284 architecture for the full 7-session period, including 800 spines for ketamine (n = 3 mice;
285 28 fields of view), and 783 spines for saline (n = 2 mice; 25 fields of view). For each field
286 of view, we counted multiple branches including dozens of dendritic spines (mean = 38
287 spines per field of view, s.d. = 17). In the first imaging session, we measured the
288 baseline dendritic spine density in MFC to be 0.28 spines per μm (mean; s.d. = 0.08; n =
289 155 fields of view). This value for dendritic spine density is ~25% lower than a previous
290 measurement from the mouse dorsomedial prefrontal cortex (Muñoz-Cuevas et al.,
291 2013), a difference that may be attributed to our mice being older adults.
292
293 Comparing between pre- and post-ketamine sessions, most dendritic spines were stable
294 (green arrowheads, **Figs. 2C and 2D**). However, there were also instances where new
295 spines were found (yellow arrowhead, **Fig. 2D**). To summarize data for ketamine and
296 saline conditions, we quantified the fold-change in dendritic spine density from baseline
297 (day -3 from injection) for each field of view. Systemic ketamine was associated with
298 higher dendritic spine density in the MFC (treatment: $p = 6 \times 10^{-7}$, $F_{1,276} = 26.0$; day: $p =$
299 0.40, $F_{5,276} = 1.03$; interaction: $p = 0.39$, $F_{5,276} = 1.05$; two-way ANOVA; **Fig. 2E**) relative
300 to the saline group. It is noteworthy that we also observed a decline in dendritic spine
301 density across days for saline-injected subjects (black line, **Fig. 2E**). This reduction of
302 spine density in "control" condition may be due to a number of factors to be discussed in
303 a later section.
304
305 **Higher dendritic spine density is driven by an elevated rate of spine formation**

306 Next we wanted to find the changes in dendritic spine turnover dynamics responsible for
307 the relative increase in dendritic spine density. Because the largest spine density
308 increase was found on the day after ketamine injection, we focused the analysis on the
309 entire data set across a period including day -3, 1, and 1 (**Fig. 3A**). **Figure 3B** shows
310 two image montages of apical tuft branches before and after ketamine injection. To
311 quantify spine turnover dynamics, we compared the same fields of view across
312 consecutive imaging sessions to count the number of new and eliminated spines.
313 Relative to pre-injection baseline, we found an increase in spine formation rate following
314 systemic ketamine, which was different from the saline group (treatment: $p = 0.03$, $F_{1,287}$
315 $= 4.61$; day: $p = 0.001$, $F_{1,287} = 10.3$; interaction: $p = 0.03$, $F_{1,287} = 4.61$; two-way ANOVA;
316 **Fig. 3C**). In contrast, although there were changes of spine elimination rates across
317 days, there was no difference between mice that received ketamine or saline (treatment:
318 $p = 0.9$, $F_{1,286} = 0.02$; day: $p = 0.003$, $F_{1,286} = 9.09$; interaction: $p = 0.9$, $F_{1,286} = 0.02$; two-
319 way ANOVA; **Fig. 3D**). We also plotted the spine turnover rates using only the 7-session
320 data set for the ketamine (**Fig. 3E**) and saline groups (**Fig. 3F**). Ketamine remained a
321 significant factor contributing to a difference in spine formation rate (treatment: $p = 2 \times$
322 10^{-4}, $F_{1,267} = 14.5$; day: $p = 0.5$, $F_{5,267} = 0.89$; interaction: $p = 0.08$, $F_{5,267} = 1.96$; two-way
323 ANOVA), but not for the spine elimination rate (treatment: $p = 0.1$, $F_{1,267} = 2.79$; day: $p =$
324 0.001, $F_{5,267} = 4.19$; interaction: $p = 0.07$, $F_{5,267} = 2.03$; two-way ANOVA). These results
325 indicate that an elevated rate of spine formation is the driving force behind the higher
326 spine density in the MFC following ketamine administration.
327
328 Although the mean spine formation rate was higher for mice with systemic ketamine
329 relative to saline, there was variability across fields of view (**Fig. 3G**). As described
330 previously, there was a decline in spine density across days in saline-injected subjects,
331 and accordingly 83% of the imaged field of dendritic tuft branches had reduced spine

332 density compared to the first-day baseline. By contrast, about half of the fields of view
333 had an increase in spine density following ketamine injection (40%; p = 0.005, chi-
334 square = 7.8, chi-square test). Using fields of view allows us to examine more finely the
335 variability in the data, however results could be correlated among fields of view from the
336 same individual. Therefore, we verified on a per-subject basis across 7 days that there is
337 a significant effect of treatment on dendritic spine density (treatment: p = 0.007, $F_{1,16}$ =
338 9.39; day: p = 0.87, $F_{5,16}$ = 0.35; interaction: p = 0.46, $F_{5,16}$ = 0.98; two-way ANOVA),
339 effect near but did not reach statistical significance for treatment on spine formation rate
340 (treatment: p = 0.07, $F_{1,16}$ = 3.87; day: p = 0.96, $F_{5,16}$ = 0.20; interaction: p = 0.69, $F_{5,16}$ =
341 0.62; two-way ANOVA), and no effect of treatment on spine elimination rate (treatment:
342 p = 0.64, $F_{1,16}$ = 0.23; day: p = 0.23, $F_{5,16}$ = 1.56; interaction: p = 0.62, $F_{5,16}$ = 0.71; two-
343 way ANOVA).
344
345 **A fraction of the newly formed spines associated with ketamine administration is**
346 **persistent**
347 An important question is whether the new dendritic spines associated with ketamine
348 administration become functional synapses. A previous study correlated images from
349 two-photon and electron microscopy to show that a fraction of the newly formed dendritic
350 spines is transient and disappears, whereas persistent spines that are stable for more
351 than 4 days had synapses (Knott et al., 2006). For the new spines that were observed
352 on the day following ketamine or saline injection, we quantified the fraction that could be
353 observed at the same location 4 days later. Across fields of view, we found no difference
354 in the fraction of spines that became persistent for ketamine versus saline (ketamine: 39
355 ± 5%, saline: 32 ± 4%, mean ± s.e.m.; p = 0.3, t_{40} = 0.99, unpaired t-test; **Fig. 4A**).
356 However, the persistent fraction decreased over longer periods for ketamine-injected
357 mice (day 5 versus day 10: p = 0.007, t_{17} = 3.08; day 5 versus day 15: p = 0.002, t_{15} =

358 3.85; paired t-test, exact p-values reported without multiple comparison adjustment),
359 whereas it was unchanged for saline-injected mice (day 5 versus day 10: p = 0.1, t_{19} =
360 1.74; day 5 versus day 15: p = 0.9, t_{12} = -0.17; paired t-test, exact p-values reported
361 without multiple comparison adjustment).
362
363 Furthermore, larger spines are known to correlate with more mature and stronger
364 synaptic connections (Kasai et al., 2003). We measured the length and width of spine
365 heads, comparing between newly formed spines and matched each of those with a
366 neighboring stable spine on the same dendritic branch. Relative to existing spines, new
367 spines that appeared immediately on the day following systemic ketamine were shorter
368 (new: 1.25 ± 0.04 μm, n = 328; existing: 1.35 ± 0.03 μm, n = 328; mean ± s.e.m.; p =
369 0.02, t_{327} = -2.39, paired t-test) and narrower (new: 0.74 ± 0.01 μm; existing: 0.83 ± 0.02
370 μm, mean ± s.e.m.; $p = 3 \times 10^{-5}$, t_{327} = -4.19, paired t-test). These differences in averages
371 were reflected as differences in the cumulative distributions as well (spine length: $p = 9 \times$
372 10^{-6}, $D_{328,328}$ = 0.19,; spine width: $p = 4 \times 10^{-4}$, $D_{328,328}$ = 0.16; two-sample Kolmogorov-
373 Smirnov test; **Figs. 4B-C**). However, when we compared pre- versus post-ketamine
374 conditions, we did not find any difference in dendritic spine morphology (spine length,
375 new spines: p = 0.9, $D_{61,328}$ = 0.08; spine length, existing spines: p = 0.09, $D_{61,328}$ = 0.17;
376 spine width, new spines: p = 0.2, $D_{61,328}$ = 0.15; spine width, existing spines: p = 0.5,
377 $D_{61,328}$ = 0.12; two-sample Kolmogorov-Smirnov test). The distributions of spine
378 protrusion length and spine head width did not suggest obvious ways to segment the
379 data, and therefore we did not attempt to identify types, i.e. stubby, mushroom, or
380 filopodia-like. Taken together, these results indicate that newly formed protrusions
381 following systemic ketamine have similar morphological characteristics to those that
382 occurred pre-ketamine. The new spine heads are shorter and narrower, broadly
383 consistent with nascent spines that precede synapse formation. Nevertheless, a fraction

384 of these spines that formed after systemic ketamine becomes persistent and likely
385 reflects new synaptic connections.
386
387 **Ketamine also leads to rapid retraction of distal apical tuft branches**
388 Unexpectedly, we also observed alterations to the distal apical tuft branches following
389 ketamine injection in a fraction (18%) of the fields of view (**Fig. 5A**). **Figure 5B** shows
390 the same field of view across imaging sessions where a distal branch segment was
391 visible in a pre-injection session (red arrowheads, **Fig. 5B**), and then disappeared on the
392 day following systemic ketamine administration. This observation was not due to out of
393 focus imaging, because we acquired volumetric image stacks where neuronal processes
394 below and above the image plane were clearly visible and stable (green arrowheads,
395 **Fig. 5B**). No additional alterations were observed in the subsequent days (**Fig. 5C**).
396 Analysis of the longitudinal data set revealed a mean change of -10 ± 3% in the total
397 length of the imaged apical tuft branches on day 1 after ketamine injection (treatment: p
398 = 1 x 10^{-12}, $F_{1,236}$ = 56.5; day: p = 0.02, $F_{5,236}$ = 2.77; interaction: p = 0.02, $F_{5,236}$ = 2.77;
399 two-way ANOVA**; Fig. 5D**). We compared fields of view with and without apical tuft
400 branch loss, and found no differences in their spine turnover rates (p = 0.2, formation; p
401 = 0.3 elimination; unpaired t-test). We also asked whether stable and retracted dendritic
402 branches had different widths, but did not find any difference (p = 0.4, t_{131} = -0.77,
403 unpaired t-test; **Fig. 5E**). Additional statistical tests on a per-subject basis for the 3-
404 session data confirmed a significant effect of treatment on apical tuft branch length
405 (treatment: p = 0.003, $F_{1,16}$ = 12.08; day: p = 0.7, $F_{5,16}$ = 0.62; interaction: p = 0.7, $F_{5,16}$ =
406 0.62; two-way ANOVA). These results show that systemic ketamine has a short-term
407 effect of removing a small portion of the apical dendritic tuft branches in layer 1.
408

409 **Potential factors contributing to the decline of dendritic spine density prior to**
410 **injection**

411 We observed a decline in dendritic spine density in saline-injected mice. To further
412 investigate the potential contributing factors, we examined changes in spine density
413 during the pre-injection period, between day -3 and -1. There were no significant
414 differences between mice to be injected with saline versus ketamine (p = 1, Wilcoxon
415 rank-sum test; **Fig. 6A**), or between male and female subjects (p = 0.3, Wilcoxon rank-
416 sum test; **Fig. 6B**). We conjecture that stress could arise from the duration of anesthesia
417 required for imaging, but found no systematic trend between imaging session duration
418 and changes in spine density (p = 0.8, t_{13} = 0.26, linear regression, excluding outlier at -
419 0.3; **Fig. 6C**). There was also no significant trend for age of the animal at the time of
420 glass window implant (p = 0.8, t_{13} = -0.23, linear regression, excluding outlier at -0.3;
421 **Fig. 6D**). A potential contributor is age of the animal at the time of imaging, where older
422 adults tended to have larger decline in dendritic spine density (p = 0.16, t_{13} = -1.50,
423 linear regression, excluding outlier at -0.3; **Fig. 6E**), although this effect did not reach
424 significance. We should note that there have been a couple of other reports of structural
425 loss in rodent prefrontal cortex in control or vehicle-injected animals (Wellman, 2001;
426 Muñoz-Cuevas et al., 2013). These earlier studies along with our own data highlight the
427 difficulty in achieving true "controls" in studies of frontal cortex, where the brain region is
428 known to be sensitive to aversive life events.
429

430 **Discussion**

431 Our time-lapse results demonstrated higher dendritic spine density for up to 2 weeks
432 after a single dose of ketamine relative to saline. This is a consequence of an elevated
433 rate of spine formation. We also observed a loss of distal apical tuft branches that was
434 specific to the day following ketamine injection. The short- and long-term effects on

435 apical tuft branches and dendritic spine density would have opposite effects on the
436 overall number of synaptic connections. By removing certain inputs immediately and
437 adding others gradually, we suggest that ketamine may act to reorganize the types of
438 synaptic inputs received by pyramidal neurons in the MFC. Physiological evidence
439 hinted at this possibility; in the frontal cortex, hypocretin-sensitive synaptic inputs
440 originate from the thalamus, likely distinct from those that mediate serotonergic
441 signaling. Intriguingly, although ketamine restores the magnitude of these synaptic
442 currents in stressed rats, they appear to reach different levels relative to baseline (Li et
443 al., 2011). Further experiments are needed to confirm the identities of the added and lost
444 synaptic connections following systemic ketamine administration.
445
446 Our study builds on previous studies of ketamine in naive rats and chronic stress
447 models, which found an increase in dendritic spine density in the distal and proximal
448 tufts of layer 5 pyramidal neurons (Li et al., 2010; 2011). These studies examined
449 structural changes in the anterior cingulate and prelimbic regions by filling cells in brain
450 slices prepared 24 hr after treatment. Here, investigating effects *in vivo*, we found a
451 relative increase in spine density in the MFC, which is more dorsally located but still part
452 of the rodent medial prefrontal cortical network (Van De Werd et al., 2010; Vogt and
453 Paxinos, 2012). We should emphasize that the observed relative increase is a result of
454 dendritic spine density remaining mostly stable for ketamine, but declining for saline-
455 injected mice. The decline of spine density in the saline group suggests that mice might
456 have been stressed inadvertently in our experiments, potentially as a function of age at
457 the time of imaging. Interestingly, other studies have observed an increase in dendritic
458 spine density following a single dose of another rapid acting antidepressant,
459 scopolamine (Voleti et al., 2013), and reversal of stress-induced atrophy by chronic
460 administration of fluoxetine (Bessa et al., 2009). Therefore, our results and studies in the

field (Bessa et al., 2009; Li et al., 2010; 2011; Voleti et al., 2013) support a structural basis for antidepressant actions that may generalize beyond specific frontal cortical regions or pharmacological agents.

A novel finding is that the higher dendritic spine density after systemic ketamine is due to an elevated spine formation rate, but not changes to the spine elimination rate. This increase in spine formation rate was largest on the day after systemic ketamine administration. For the later imaging sessions, spine formation rate remained above the baseline, pre-injection levels. This time course of elevated spine formation rate may be compared to the time course of the antidepressant effects of systemic ketamine. In rats, depressive-like behaviors as assayed by forced swim and sucrose preference tests were reduced 1 week after injection of ketamine (Autry et al., 2011; Li et al., 2011). In patients with major depressive disorder, the duration of ketamine's antidepressant effects varies from 3 days to 2 weeks (Ibrahim et al., 2012). Therefore, the long-term effect on dendritic spine turnover may relate to the sustained antidepressant effects observed in rodents and humans. Furthermore, the observation of dynamics changes in spine formation rate, but not other structural plasticity parameters, suggests that antidepressant effects may rely on molecular pathways that promote synaptogenesis, rather than those related to spine growth or pruning.

Several factors may influence the rates of ketamine-induced structural remodeling. Sex is a contributing variable because estrogen is known to affect structural plasticity (Srivastava et al., 2008). In this study, sex differences were not tested explicitly owing to the limited sample size. Two lines of evidence suggest that pooling the data from males and females should not affect the conclusions of this study. First, we repeated the analysis using data from the 5 ketamine-injected males only, and found similar trends for

487 ketamine-induced changes, including relative increase in dendritic spine density,
488 elevated spine formation rate, but no change in spine elimination rate. Second, two
489 recent studies reported that although female rats are more sensitive to the
490 antidepressant-like effects of ketamine at low dose, behavioral outcomes are similar
491 between males and females at higher doses (Carrier and Kabbaj, 2013; Franceschelli et
492 al., 2015). Here, we used a dose (10 mg/kg) at which these studies found comparable
493 behavioral effects for the sexes. Another potential variable is surgical method. One
494 report argued that open-skull craniotomy can alter dendritic spine turnover rates (Xu et
495 al., 2007), although another study found negligible differences across surgical
496 preparations (Holtmaat et al., 2009). The same procedures were applied to the ketamine
497 and saline groups in our study; therefore the influence of surgical methods on the
498 across-group differences should be minimal. Furthermore, ketamine is often used with
499 xylazine as an anesthetic. There is evidence that an anesthetic dose of ketamine has
500 transient effects on the dynamics of dendritic filopodia but no effect on dendritic spines in
501 1 month old mice (Yang et al., 2011). It is unclear how this prior result compares with the
502 current findings, because we used a subanesthetic dose.
503
504 A surprising observation was the retraction of distal apical tuft branches, specific to the
505 day after systemic ketamine administration. We emphasize that the imaged branch
506 segments reside in the superficial layers of the cortex, therefore representing the distal
507 portion and only a tiny fraction of the entire dendritic tree of a neuron. The loss of apical
508 tuft branch tips may be due to retraction of dendritic branches or death of neurons from
509 which these dendrites arise, possibilities that could not be distinguished from our data.
510 Nevertheless, our result was unexpected because although some cortical cell types such
511 as GABAergic interneurons can undergo branch tip reorganization under certain
512 conditions (Chen et al., 2011), the dendritic branches of pyramidal neurons are thought

513 to be remarkably stable in the neocortex of adult mice (Grutzendler et al., 2002). Studies
514 have shown that structural plasticity in MFC is important for cognitive behaviors such as
515 consolidation of contextual memory (Vetere et al., 2011) and adaptive decision-making
516 (Liston et al., 2006; Dias-Ferreira et al., 2009). Therefore, loss of dendritic materials may
517 contribute to cognitive impairments, which are known to affect chronic ketamine users
518 (Morgan et al., 2009). At higher dosage, repeated ketamine use has been associated
519 with reduced volume of hippocampus and frontal lobe in humans (Liao et al., 2011) and
520 rodents (Kassem et al., 2013; Schobel et al., 2013). One correlated functional imaging
521 study showed that such grey matter reduction is primarily due to a loss of dendrites and
522 their synapses (Kassem et al., 2013). There are ongoing efforts in the field to develop
523 compounds with ketamine-like antidepressant actions but without the psychotomimetic
524 effects, and it would be interesting to test whether those drugs may promote structural
525 plasticity but spare dendritic material loss.
526
527 The short- and long-term effects of distal tuft branch loss and elevated spine formation
528 rate have opposing effects on the total number of dendritic spines in the MFC. Long-
529 range inputs into the superficial layers of rodent MFC come from multiple sources
530 including mediodorsal and midline thalamic nuclei, basolateral amygdala, and other
531 prefrontal cortical areas (Hoover and Vertes, 2007; Oh et al., 2014). Specific types of
532 prefrontal cortical inputs and outputs may be more plastic and susceptible to stress or
533 ketamine (Shansky et al., 2009; Liu et al., 2015). Therefore, approaches that can alter
534 prefrontal cortical circuitry with pathway specificity may be effective treatment options for
535 mood disorders and merit further study.
536
537

538 **References**

539 Autry AE, Adachi M, Nosyreva E, Na ES, Los MF, Cheng P-F, Kavalali ET, Monteggia
540 LM (2011) NMDA receptor blockade at rest triggers rapid behavioural
541 antidepressant responses. Nature 475:91–95.

542 Berman RM, Cappiello A, Anand A, Oren DA, Heninger GR, Charney DS, Krystal JH
543 (2000) Antidepressant effects of ketamine in depressed patients. Biol Psychiatry
544 47:351–354.

545 Bessa JM, Ferreira D, Melo I, Marques F, Cerqueira JJ, Palha JA, Almeida OFX, Sousa
546 N (2009) The mood-improving actions of antidepressants do not depend on
547 neurogenesis but are associated with neuronal remodeling. Mol Psychiatry 14:764–
548 73–739.

549 Carrier N, Kabbaj M (2013) Sex differences in the antidepressant-like effects of
550 ketamine. Neuropharmacology 70:27–34.

551 Cerqueira JJ, Taipa R, Uylings HBM, Almeida OFX, Sousa N (2007) Specific
552 configuration of dendritic degeneration in pyramidal neurons of the medial prefrontal
553 cortex induced by differing corticosteroid regimens. Cereb Cortex 17:1998–2006.

554 Chen JL, Lin WC, Cha JW, So PT, Kubota Y, Nedivi E (2011) Structural basis for the
555 role of inhibition in facilitating adult brain plasticity. Nat Neurosci 14:587–594.

556 Christoffel DJ, Golden SA, Russo SJ (2011) Structural and synaptic plasticity in stress-
557 related disorders. Rev Neurosci 22:535–549.

558 Cook SC, Wellman CL (2004) Chronic stress alters dendritic morphology in rat medial
559 prefrontal cortex. J Neurobiol 60:236–248.

560 Dias-Ferreira E, Sousa JC, Melo I, Morgado P, Mesquita AR, Cerqueira JJ, Costa RM,
561 Sousa N (2009) Chronic stress causes frontostriatal reorganization and affects
562 decision-making. Science 325:621–625.

563 Donahue RJ, Muschamp JW, Russo SJ, Nestler EJ, Carlezon WA (2014) Effects of
564 striatal ΔFosB overexpression and ketamine on social defeat stress-induced
565 anhedonia in mice. Biol Psychiatry 76:550–558.

566 Drevets WC, Price JL, Simpson JR, Todd RD, Reich T, Vannier M, Raichle ME (1997)
567 Subgenual prefrontal cortex abnormalities in mood disorders. Nature 386:824–827.

568 Duman RS, Aghajanian GK (2012) Synaptic dysfunction in depression: potential
569 therapeutic targets. Science 338:68–72.

570 Duncan GE, Miyamoto S, Leipzig JN, Lieberman JA (1999) Comparison of brain
571 metabolic activity patterns induced by ketamine, MK-801 and amphetamine in rats:
572 support for NMDA receptor involvement in responses to subanesthetic dose of
573 ketamine. Brain Res 843:171–183.

574 Feng G, Mellor RH, Bernstein M, Keller-Peck C, Nguyen QT, Wallace M, Nerbonne JM,

575 Lichtman JW, Sanes JR (2000) Imaging neuronal subsets in transgenic mice
576 expressing multiple spectral variants of GFP. Neuron 28:41–51.

577 Franceschelli A, Sens J, Herchick S, Thelen C, Pitychoutis PM (2015) Sex differences in
578 the rapid and the sustained antidepressant-like effects of ketamine in stress-naïve
579 and "depressed" mice exposed to chronic mild stress. Neuroscience 290:49–60.

580 Fu M, Yu X, Lu J, Zuo Y (2012) Repetitive motor learning induces coordinated formation
581 of clustered dendritic spines in vivo. Nature 483:92–95.

582 Fuchikami M, Thomas A, Liu R, Wohleb ES, Land BB, DiLeone RJ, Aghajanian GK,
583 Duman RS (2015) Optogenetic stimulation of infralimbic PFC reproduces ketamine's
584 rapid and sustained antidepressant actions. PNAS 112:8106–8111.

585 Grutzendler J, Kasthuri N, Gan W-B (2002) Long-term dendritic spine stability in the
586 adult cortex. Nature 420:812–816.

587 Holtmaat A, Bonhoeffer T, Chow DK, Chuckowree J, De Paola V, Hofer SB, Hübener M,
588 Keck T, Knott G, Lee W-CA, Mostany R, Mrsic-Flogel TD, Nedivi E, Portera-Cailliau
589 C, Svoboda K, Trachtenberg JT, Wilbrecht L (2009) Long-term, high-resolution
590 imaging in the mouse neocortex through a chronic cranial window. Nature Protocols
591 4:1128–1144.

592 Hoover WB, Vertes RP (2007) Anatomical analysis of afferent projections to the medial
593 prefrontal cortex in the rat. Brain Struct Funct 212:149–179.

594 Ibrahim L, DiazGranados N, Franco-Chaves J, Brutsche N, Henter ID, Kronstein P,
595 Moaddel R, Wainer I, Luckenbaugh DA, Manji HK, Zarate CA (2012) Course of
596 improvement in depressive symptoms to a single intravenous infusion of ketamine
597 vs add-on riluzole: results from a 4-week, double-blind, placebo-controlled study.
598 Neuropsychopharmacology 37:1526–1533.

599 Ito H, Nagano M, Suzuki H, Murakoshi T (2010) Chronic stress enhances synaptic
600 plasticity due to disinhibition in the anterior cingulate cortex and induces hyper-
601 locomotion in mice. Neuropharmacology 58:746–757.

602 Kang HJ, Voleti B, Hajszan T, Rajkowska G, Stockmeier CA, Licznerski P, Lepack A,
603 Majik MS, Jeong LS, Banasr M, Son H, Duman RS (2012) Decreased expression of
604 synapse-related genes and loss of synapses in major depressive disorder. Nature
605 Medicine 18:1413–1417.

606 Kasai H, Matsuzaki M, Noguchi J, Yasumatsu N, Nakahara H (2003) Structure-stability-
607 function relationships of dendritic spines. Trends in Neurosciences 26:360–368.

608 Kassem MS, Lagopoulos J, Stait-Gardner T, Price WS, Chohan TW, Arnold JC, Hatton
609 SN, Bennett MR (2013) Stress-induced grey matter loss determined by MRI is
610 primarily due to loss of dendrites and their synapses. Mol Neurobiol 47:645–661.

611 Kim Y, Perova Z, Mirrione MM, Pradhan K, Henn FA, Shea S, Osten P, Li B (2016)
612 Whole-brain mapping of neuronal activity in the learned helplessness model of
613 depression. Front Neural Circuits 10:3.

614 Knott GW, Holtmaat A, Wilbrecht L, Welker E, Svoboda K (2006) Spine growth precedes
615 synapse formation in the adult neocortex in vivo. Nat Neurosci 9:1117–1124.

616 Lai CSW, Franke TF, Gan W-B (2013) Opposite effects of fear conditioning and
617 extinction on dendritic spine remodelling. Nature 482:87–91.

618 Li N, Lee B, Liu R-J, Banasr M, Dwyer JM, Iwata M, Li X-Y, Aghajanian G, Duman RS
619 (2010) mTOR-dependent synapse formation underlies the rapid antidepressant
620 effects of NMDA antagonists. Science 329:959–964.

621 Li N, Liu R-J, Dwyer JM, Banasr M, Lee B, Son H, Li X-Y, Aghajanian G, Duman RS
622 (2011) Glutamate N-methyl-D-aspartate receptor antagonists rapidly reverse
623 behavioral and synaptic deficits caused by chronic stress exposure. Biol Psychiatry
624 69:754–761.

625 Liao Y, Tang J, Corlett PR, Wang X, Yang M, Chen H, Liu T, Chen X, Hao W, Fletcher
626 PC (2011) Reduced dorsal prefrontal gray matter after chronic ketamine use. Biol
627 Psychiatry 69:42–48.

628 Liston C, Gan W-B (2011) Glucocorticoids are critical regulators of dendritic spine
629 development and plasticity in vivo. PNAS 108:16074–16079.

630 Liston C, Miller MM, Goldwater DS, Radley JJ, Rocher AB, Hof PR, Morrison JH,
631 McEwen BS (2006) Stress-induced alterations in prefrontal cortical dendritic
632 morphology predict selective impairments in perceptual attentional set-shifting. J
633 Neurosci 26:7870–7874.

634 Liu R-J, Fuchikami M, Dwyer JM, Lepack AE, Duman RS, Aghajanian GK (2013) GSK-3
635 inhibition potentiates the synaptogenic and antidepressant-like effects of
636 subthreshold doses of ketamine. Neuropsychopharmacology 38:2268–2277.

637 Liu R-J, Ota KT, Dutheil S, Duman RS, Aghajanian GK (2015) Ketamine Strengthens
638 CRF-Activated Amygdala Inputs to Basal Dendrites in mPFC Layer V Pyramidal
639 Cells in the Prelimbic but not Infralimbic Subregion, A Key Suppressor of Stress
640 Responses. Neuropsychopharmacology 40:2066–2075.

641 Miyamoto S, Leipzig JN, Lieberman JA, Duncan GE (2000) Effects of ketamine, MK-801,
642 and amphetamine on regional brain 2-deoxyglucose uptake in freely moving mice.
643 Neuropsychopharmacology 22:400–412.

644 Morgan CJA, Muetzelfeldt L, Curran HV (2009) Ketamine use, cognition and
645 psychological wellbeing: a comparison of frequent, infrequent and ex-users with
646 polydrug and non-using controls. Addiction 104:77–87.

647 Muñoz-Cuevas FJ, Athilingam J, Piscopo D, Wilbrecht L (2013) Cocaine-induced
648 structural plasticity in frontal cortex correlates with conditioned place preference. Nat
649 Neurosci 16:1367–1369.

650 Oh SW et al. (2014) A mesoscale connectome of the mouse brain. Nature 508:207–214.

651 Pologruto TA, Sabatini BL, Svoboda K (2003) ScanImage: flexible software for operating

652 laser scanning microscopes. Biomed Eng Online 2:13.

653 Radley JJ, Rocher AB, Miller M, Janssen WGM, Liston C, Hof PR, McEwen BS,
654 Morrison JH (2006) Repeated stress induces dendritic spine loss in the rat medial
655 prefrontal cortex. Cereb Cortex 16:313–320.

656 Radley JJ, Sisti HM, Hao J, Rocher AB, McCall T, Hof PR, McEwen BS, Morrison JH
657 (2004) Chronic behavioral stress induces apical dendritic reorganization in pyramidal
658 neurons of the medial prefrontal cortex. Neuroscience 125:1–6.

659 Ruddy RM, Chen Y, Milenkovic M, Ramsey AJ (2015) Differential effects of NMDA
660 receptor antagonism on spine density. Synapse 69:52–56.

661 Sanacora G, Schatzberg AF (2015) Ketamine: promising path or false prophecy in the
662 development of novel therapeutics for mood disorders? Neuropsychopharmacology
663 40:259–267.

664 Schneider CA, Rasband WS, Eliceiri KW (2012) NIH Image to ImageJ: 25 years of
665 image analysis. Nature Methods 9:671–675.

666 Schobel SA, Chaudhury NH, Khan UA, Paniagua B, Styner MA, Asllani I, Inbar BP,
667 Corcoran CM, Lieberman JA, Moore H, Small SA (2013) Imaging patients with
668 psychosis and a mouse model establishes a spreading pattern of hippocampal
669 dysfunction and implicates glutamate as a driver. Neuron 78:81–93.

670 Shansky RM, Hamo C, Hof PR, McEwen BS, Morrison JH (2009) Stress-induced
671 dendritic remodeling in the prefrontal cortex is circuit specific. Cereb Cortex
672 19:2479–2484.

673 Srivastava DP, Woolfrey KM, Woolfrey K, Jones KA, Shum CY, Lash LL, Swanson GT,
674 Penzes P (2008) Rapid enhancement of two-step wiring plasticity by estrogen and
675 NMDA receptor activity. PNAS 105:14650–14655.

676 Thévenaz P, Ruttimann UE, Unser M (1998) A pyramid approach to subpixel registration
677 based on intensity. Image Processing, IEEE Transactions on 7:27–41.

678 Trachtenberg JT, Chen BE, Knott GW, Feng G, Sanes JR, Welker E, Svoboda K (2002)
679 Long-term in vivo imaging of experience-dependent synaptic plasticity in adult
680 cortex. Nature 420:788–794.

681 US Burden of Disease Collaborators (2013) The state of US health, 1990-2010: burden
682 of diseases, injuries, and risk factors. JAMA 310:591–608.

683 Van De Werd HJJM, Rajkowska G, Evers P, Uylings HBM (2010) Cytoarchitectonic and
684 chemoarchitectonic characterization of the prefrontal cortical areas in the mouse.
685 Brain Struct Funct 214:339–353.

686 Vetere G, Restivo L, Cole CJ, Ross PJ, Ammassari-Teule M, Josselyn SA, Frankland
687 PW (2011) Spine growth in the anterior cingulate cortex is necessary for the
688 consolidation of contextual fear memory. PNAS 108:8456–8460.

689 Vogt BA, Paxinos G (2012) Cytoarchitecture of mouse and rat cingulate cortex with
690 human homologies. Brain Struct Funct 219:185–192.

691 Voleti B, Navarria A, Liu R-J, Banasr M, Li N, Terwilliger R, Sanacora G, Eid T,
692 Aghajanian G, Duman RS (2013) Scopolamine Rapidly Increases Mammalian
693 Target Of Rapamycin Complex 1 Signaling, Synaptogenesis, and Antidepressant
694 Behavioral Responses. Biol Psychiatry:1–8.

695 Wellman CL (2001) Dendritic reorganization in pyramidal neurons in medial prefrontal
696 cortex after chronic corticosterone administration. J Neurobiol 49:245–253.

697 Xu H-T, Pan F, Yang G, Gan W-B (2007) Choice of cranial window type for in vivo
698 imaging affects dendritic spine turnover in the cortex. Nat Neurosci 10:549–551.

699 Yang G, Chang PC, Bekker A, Blanck TJJ, Gan W-B (2011) Transient effects of
700 anesthetics on dendritic spines and filopodia in the living mouse cortex.
701 Anesthesiology 115:718–726.

702

703

Figures and Legends

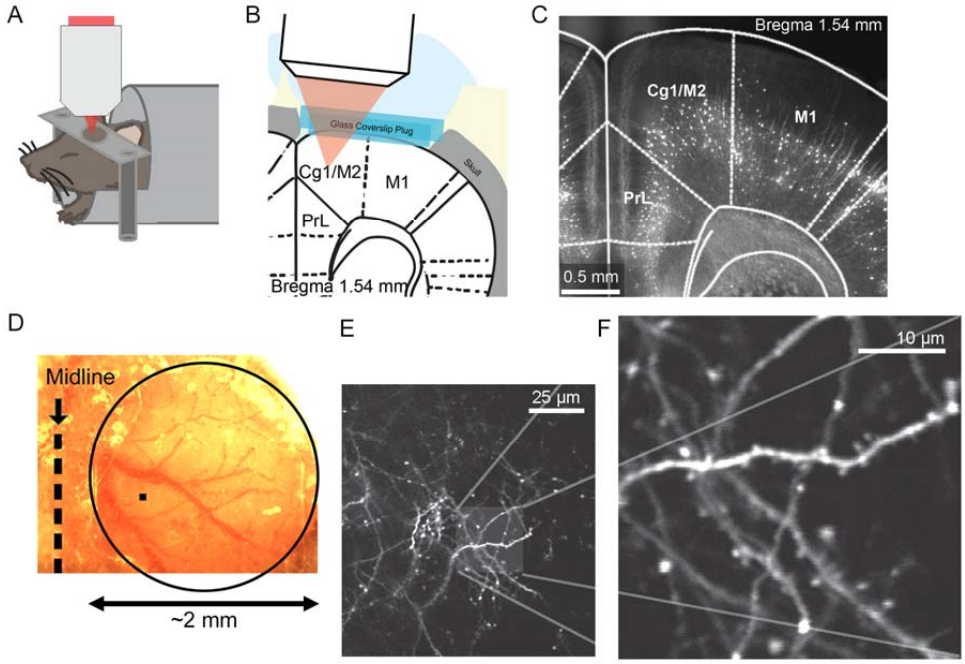

Figure 1: Longitudinal imaging of dendritic architecture in the mouse medial frontal cortex.

(**A**) Schematic of the imaging experiment.

(**B**) Schematic of the chronic window implant.

(**C**) Fluorescence image of a fixed coronal brain slice from a *Thy1-GFP-M* mouse following longitudinal imaging. Cg1/M2, cingulate and medial secondary motor regions, i.e. the medial frontal cortex (MFC) that was imaged in this study. PrL, prelimbic cortex. M1, primary motor cortex.

(**D**) Bright-field image of the chronic window implant. The glass window is ~2-mm diameter wide (circle), which is much larger than the imaging field of view, ~60 x 60 µm (filled square).

(**E**) A low-magnification, *in vivo* two-photon image from layer 1 of the MFC in a *Thy1-GFP-M* mouse. Distal apical tuft branches from GFP-expressing layer 5 pyramidal neurons were visible.

(**F**) A high-magnification image of a region in (E).

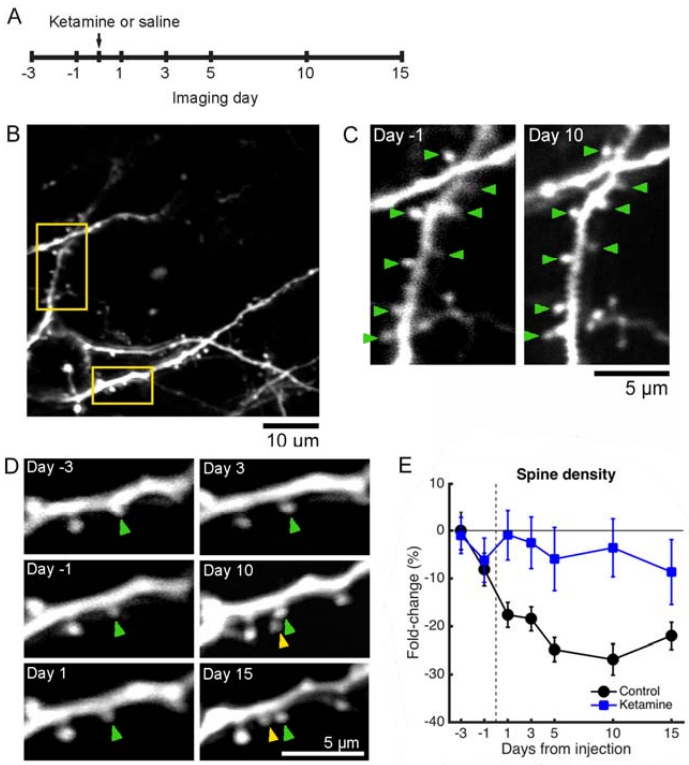

Figure 2: Systemic ketamine leads to higher dendritic spine density for at least 2 weeks relative to controls

(**A**) Time line of the experiment. Ketamine was administered at a dose of 10 mg/kg through i.p. injection.

(**B**) An example imaging field of view acquired on day -3 in a *Thy1-GFP-M* mouse. Yellow boxes indicate the dendritic branches shown as examples in panels C and D.

(**C**) Images of an apical dendritic tuft branch at -1 and 10 day from ketamine administration in a *Thy1-GFP-M* mouse. In the bottom right, axonal processes and boutons are visible. Green arrowhead, stable spine.

(**D**) Another apical dendritic tuft branch from the same field of view at -3, -1, 1, 3, 10, and 15 day from ketamine administration in a *Thy1-GFP-M* mouse. A new spine (yellow arrowhead) appeared on day 10 next to a stable spine (green arrowhead).

737 (**E**) Change in dendritic spine density across days, expressed as fold-change from the
738 value measured on the first imaging session. The mouse was injected with either
739 ketamine (blue square) or saline (black circle). Mean ± s.e.m. N = 28 and 25 fields of
740 view across 7 sessions for ketamine- and saline-injected mice.
741
742

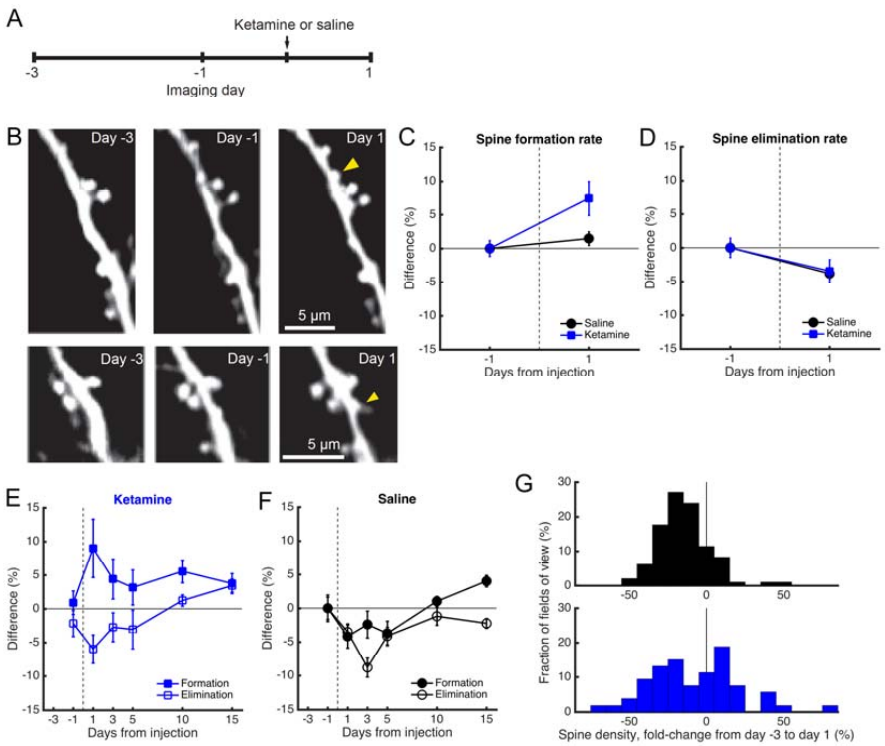

Figure 3: Higher spine density is due to an elevated rate of spine formation

(**A**) Time line of the experiment. Ketamine was administered at a dose of 10 mg/kg through i.p. injection.

(**B**) Images of two different apical dendritic tuft branches at -3, -1, and 1 day from ketamine administration in a *Thy1-GFP-M* mouse. Yellow arrowhead, new spine.

(**C**) Change in spine formation rate, expressed as difference from the value measured between day -3 and -1, i.e. pre-injection sessions. The mouse was injected with either ketamine (blue square) or saline (black circle). Mean ± s.e.m. N = 58 and 97 fields of view across 3 sessions for ketamine- and saline-injected mice.

(**D**) Same as (C) for spine elimination rate.

(**E**) Change in spine turnover dynamics across days for mice injected with ketamine. Solid square, spine formation rate. Open square, spine elimination rate. Mean ± s.e.m.

(**F**) Same as (F) for controls with saline injection. N = 28 and 25 fields of view across 7 sessions for ketamine- and saline-injected mice.

(**G**) A histogram of the change in dendritic spine density, expressed as fold-change from day -3 to day 1 from injection. Top, saline. Bottom, ketamine. N = 58 and 97 fields of view for ketamine- and saline-injected mice.

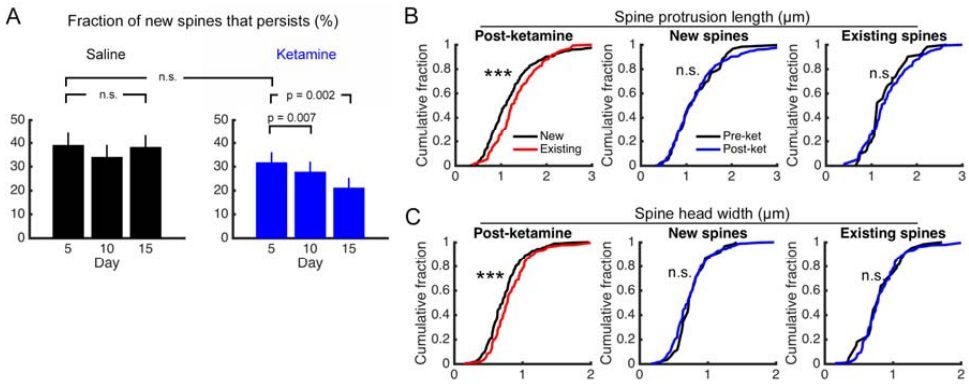

Figure 4: Newly formed protrusions following systemic ketamine are consistent with nascent spines

(A) The fraction of newly formed spines found on day 1 that could be observed again on day 5, 10, or 15, for mice injected with saline (black) or ketamine (blue). Paired t-test for comparisons across days in same condition. Unpaired t-test for the comparison across conditions. P-values are shown as is without multiple comparison correction. Mean ± s.e.m. N = 28 and 25 fields of view for ketamine- and saline-injected mice.

(**B**) Distribution of spine protrusion lengths, comparing between newly formed spines and existing, stable spines that were on the same dendritic branch. Measurements were taken either pre-ketamine, on day -1, or post-ketamine, on day 1, 3, 5, 10, or 15. ***, $p<0.001$, two-sample Kolmogorov-Smirnov test. N = 61 new spines and 61 matched, existing neighboring spines measured pre-ketamine. N = 328 new spines and 328 matched, existing neighboring spines measured post-ketamine.

(**C**) Same as (B) for spine head widths.

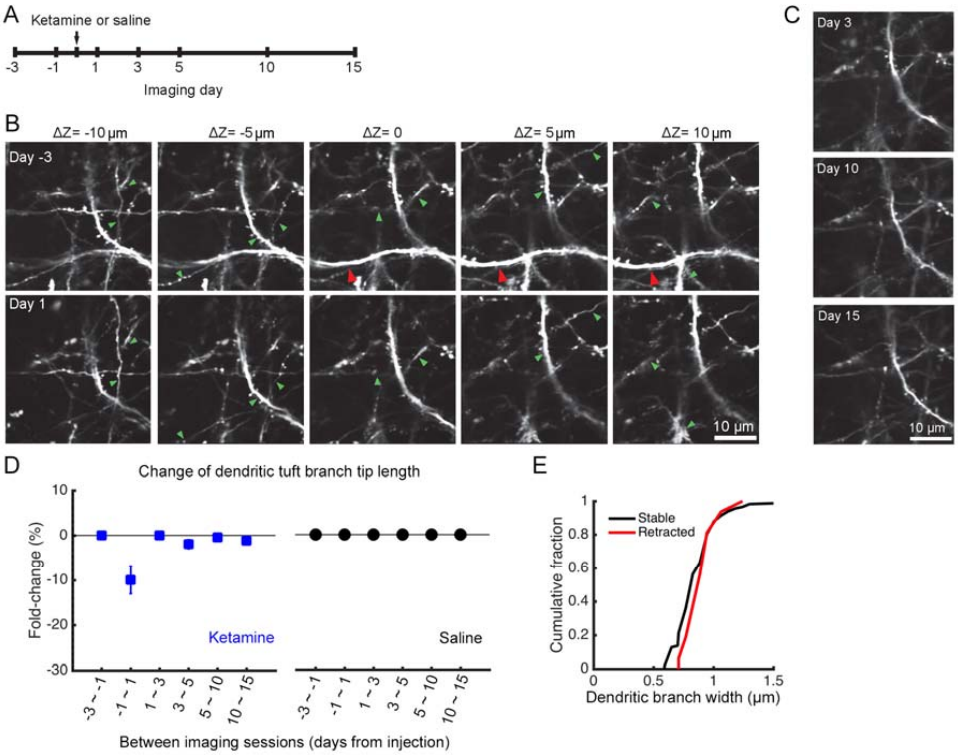

Figure 5: Systemic ketamine associated with retraction of distal apical tuft branches

(**A**) Time line of the experiment. Ketamine was administered at a dose of 10 mg/kg through i.p. injection.

(**B**) Images from multiple z-depths of a volumetric acquisition of dendritic architecture obtained in a *Thy1-GFP-M* mouse before and after ketamine administration. Note that although most branch segments were stable (green arrowhead), a segment in the middle of the volume has retracted (red arrowhead).

(**C**) Same field of view as (B) at 3, 10, and 15 day from ketamine administration.

(**D**) Change in distal apical tuft branch length in layer 1 across days, with fold-change calculated by dividing the length of each session by that from the prior session. The mouse was injected with either ketamine (blue square) or saline vehicle (black circles).

794 Mean ± s.e.m. N = 28 and 25 fields of view across 7 sessions for ketamine- and saline-
795 injected mice.
796 (**E**) Distributions of dendritic branch widths measured on day -1, plotted separately for
797 those distal apical tuft branches that were stable (black) or retracted (red) on day 1. N =
798 117 stable and 16 retracted dendritic segments from ketamine-injected mice.
799

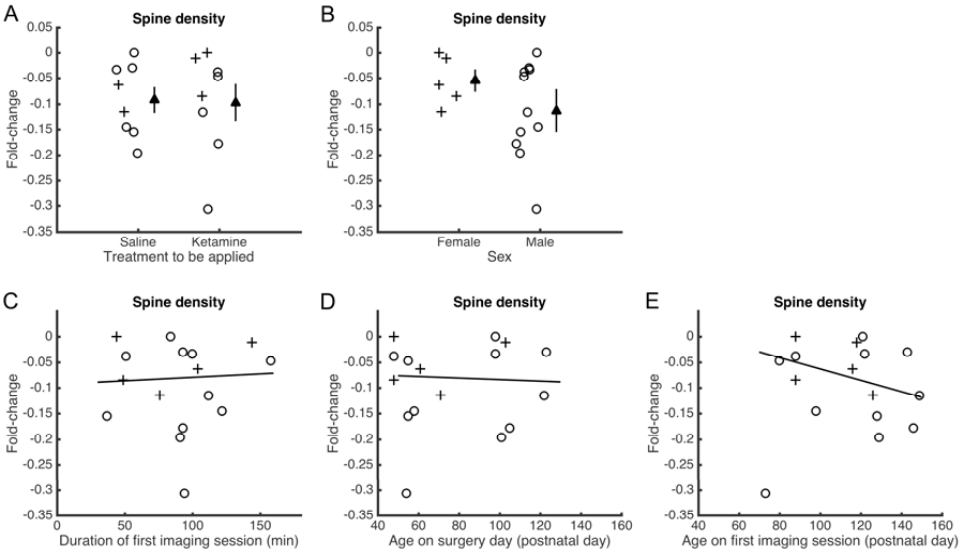

Figure 6: Potential factors contributing to the decline of dendritic spine density prior to injection

(**A**) Fold-change in dendritic spine density from day -3 to day -1 (pre-injection) for mice to be injected with saline or ketamine. Circle, male. Cross, female. Filled triangle, mean ± s.e.m.

(**B**) Same as (A) for female versus male mice.

(**C**) Fold-change in dendritic spine density from day -3 to day -1 (pre-injection) plotted as a function of the duration of the imaging session on day -3. Circle, male. Cross, female. Line, linear fit excluding the outlier at -0.3.

(**D**) Same as (C) for age at the time of surgery.

(**E**) Same as (C) for age at the time of first imaging session.

814 **Statistical Table**

		Data structure	Test	Exact *p* value	N
a	Spine density	Two-factor, btw (treatment) and win (day)	rANOVA	treatment: p = 6 x 10^{-7}; day: p = 0.40; interaction: p = 0.39	28/25 fields of view for 7 sessions for ket vs. saline
b	Spine formation rate	Two-factor, btw (treatment) and win (day)	rANOVA	treatment: p = 0.03; day: p = 0.001; interaction: p = 0.03	58/97 fields of view for 3 sessions for ket vs. saline
c	Spine elimination rate	Two-factor, btw (treatment) and win (day)	rANOVA	treatment: p = 0.9; day: p = 0.003; interaction: p = 0.9	58/97 fields of view for 3 sessions for ket vs. saline
d	Spine formation rate	Two-factor, btw (treatment) and win (day)	rANOVA	treatment: p = 2 x 10^{-4}; day: p = 0.5; interaction: p = 0.08	28/25 fields of view for 7 sessions for ket vs. saline
e	Spine elimination rate	Two-factor, btw (treatment) and win (day)	rANOVA	treatment: p = 0.1; day: p = 0.001; interaction: p = 0.07	28/25 fields of view for 7 sessions for ket vs. saline
f	Field of view fraction	Normally distributed	Chi-squared test	p = 0.005	58/97 fields of view for ket vs. saline
g	Spine density	Two-factor, btw (treatment) and win (day)	rANOVA	treatment: p = 0.007; day: p = 0.87; interaction: p = 0.98	8/8 mice for ket vs. saline
h	Spine formation rate	Two-factor, btw (treatment) and win (day)	rANOVA	treatment: p = 0.07; day: p = 0.20; interaction: p = 0.69	8/8 mice for ket vs. saline
i	Spine elimination rate	Two-factor, btw (treatment) and win (day)	rANOVA	treatment: p = 0.64; day: p = 0.23; interaction: p = 0.62	8/8 mice for ket vs. saline
j	Persistent fraction	Normally distributed	Two-tailed t-test	p = 0.3	28/25 fields of view for ket vs. saline
k	Persistent fraction	Normally distributed	Two-tailed paired t-test	p = 0.007	28 fields of view for ket

m	Persistent fraction	Normally distributed	Two-tailed paired t-test	$p = 0.002$	28 fields of view for ket
n	Persistent fraction	Normally distributed	Two-tailed paired t-test	$p = 0.1$	25 fields of view for saline
o	Persistent fraction	Normally distributed	Two-tailed paired t-test	$p = 0.9$	25 fields of view for saline
p	Spine head length	Normally distributed	Two-tailed paired t-test	$p = 0.02$	328/328 new vs. existing spines
q	Spine head width	Normally distributed	Two-tailed paired t-test	$p = 3 \times 10^{-5}$	328/328 new vs. existing spines
r	Spine head length	Cumulative fractions	Two-sample Kolmogorov -Smirnov test	$p = 9 \times 10^{-6}$	328/328 new vs. existing spines
s	Spine head width	Cumulative fractions	Two-sample Kolmogorov -Smirnov test	$p = 4 \times 10^{-4}$	328/328 new vs. existing spines
t	Spine head length	Cumulative fractions	Two-sample Kolmogorov -Smirnov test	$p = 0.9$	61/328 spines for pre- vs. post-ket
u	Spine head length	Cumulative fractions	Two-sample Kolmogorov -Smirnov test	$p = 0.09$	61/328 spines for pre- vs. post-ket
v	Spine head width	Cumulative fractions	Two-sample Kolmogorov -Smirnov test	$p = 0.2$	61/328 spines for pre- vs. post-ket
w	Spine head width	Cumulative fractions	Two-sample Kolmogorov -Smirnov test	$p = 0.5$	61/328 spines for pre- vs. post-ket
x	Dendrite length	Two-factor, btw (treatment) and win (day)	rANOVA	treatment: $p = 1 \times 10^{-12}$; day: $p = 0.02$; interaction: $p = 0.02$	28/25 fields of view for 7 sessions for ket vs. saline
y	Dendrite length and formation rate	Two variables: binary (with or without branch loss) and continuous	Regression coefficient	$p = 0.2$	28 fields of view for ket

		(formation rate)			
z	Dendrite length and elimination rate	Two variables: binary (with or without branch loss) and continuous (elimination rate)	Regression coefficient	p = 0.3	28 fields of view for ket
aa	Branch width of imaged dendritic segments	Normally distributed	Two-tailed t-test	p = 0.44	117 stable and 16 retracted dendritic segments
ab	Dendrite length	Two-factor, btw (treatment) and win (day)	rANOVA	treatment: p = 0.003; day: p = 0.69; interaction: p = 0.69	8/8 mice for ket vs. saline
ac	Change in dendritic spine density	Non-parametric	Wilcoxon ranked-sum	p = 1	8/8 mice for ket vs. saline
ad	Change in dendritic spine density	Non-parametric	Wilcoxon ranked-sum	p = 0.3	5 female and 11 male mice
ae	Change in dendritic spine density	Two continuous variables	Regression coefficient	p = 0.8	16 mice
af	Change in dendritic spine density	Two continuous variables	Regression coefficient	p = 0.8	16 mice
ag	Change in dendritic spine density	Two continuous variables	Regression coefficient	p = 0.16	16 mice

rANOVA, repeated measures analysis of variance; Btw, between-factor of the ANOVA; win, within-factor of the ANOVA.